

# Ly $\alpha$ emitters in the GOODS-S field

## A powerful pure nebular SED with N IV] emission at $z = 5.563$ \*

A. Raiter<sup>1</sup>, R. A. E. Fosbury<sup>2</sup>, and H. Teimoorinia<sup>1,3</sup>

<sup>1</sup> European Southern Observatory, Karl-Schwarzschild-Strasse 2, Garching bei München 85748, Germany  
e-mail: araiter@eso.org

<sup>2</sup> ST-ECF, Karl-Schwarzschild Str. 2, Garching bei München 85748, Germany

<sup>3</sup> Institute for Advanced Studies in Basic Sciences, PO Box 45195-1159, Zanjan 45195, Iran

Received 6 May 2009 / Accepted 17 December 2009

### ABSTRACT

**Context.** The Great Observatories Origins Deep Survey (GOODS) has provided us with one of the deepest multi-wavelength views of the distant universe. The combination of multi-band photometry and optical spectroscopy has resulted in the identification of sources whose redshifts extend to values in excess of six. Amongst these distant sources are Ly $\alpha$  emitters whose nature must be deduced by clearly identifying the different components that contribute to the measured SED.

**Aims.** From a sample of Ly $\alpha$  emitters in the GOODS-S field with uncontaminated photometry and optical (red) spectroscopy, we select a spatially compact object at a redshift of 5.563 (Ly $\alpha$ ) that shows a second emission line, identified as N IV] 1486 Å. The SED is modelled in a way that accounts for both the N IV] line emission and the photometry in a self-consistent way.

**Methods.** The photoionization code CLOUDY is used to calculate a range of nebular models as a function of stellar ionizing source temperature, ionization parameter, density and nebular metallicity. We compare the theoretical and observed magnitudes and search for the model parameters that also reproduce the observed N IV] luminosity and equivalent width.

**Results.** A nebular model with a hot blackbody ionizing source of around 100 kK and a nebular metallicity of  $\sim 5\%$  of solar is able to fit the observed SED and, in particular, explain the large apparent Balmer break which is inferred from the pure stellar population model fitting conventionally applied to multi-band photometric observations. In our model, an apparent spectral break is produced by strong [O III] 4959, 5007 Å emission falling in one of the IR bands (IRAC1 in this case). A lower limit on the total baryonic mass of a model of this type is  $3.2 \times 10^8 M_{\odot}$ .

**Conclusions.** It is argued that objects with Ly $\alpha$  emission at high redshift that show an apparent Balmer break may have their SED dominated by nebular emission and so could possibly be identified with very young starbursting galaxies rather than massive evolved stellar populations. Detailed studies of these emission nebulae with large telescopes will provide a unique insight into very early chemical evolution.

**Key words.** early Universe – Galaxy: formation – galaxies: photometry – galaxies: starburst – galaxies: stellar content – ISM: abundances

## 1. Introduction

The Ly $\alpha$  emission line is a beacon that can be recognised from the ground in objects with redshifts larger than about 1.8. When seen on its own, its interpretation is complicated by radiative transfer effects both within the emission region itself and in the intervening Lyman forest. With the detection of other emission lines and/or a recognisable continuum, a spectrum can however provide a rich source of information about physical conditions and chemical composition. Of particular interest for the identification of primordial starforming objects are the so-called “dual-emitters”: sources that emit both Ly $\alpha$  and the He II line

at 1640 Å (Dawson et al. 2004; Nagao et al. 2005; Ouchi et al. 2008) which are interpreted as very metal-poor nebulae ionized by massive, hot and presumably metal-free stars. So far, intermediate band imaging surveys have not been very successful in discovering genuine, stellar-ionized H/He II dual emitters (Nagao et al. 2008).

The Great Observatories Origins Deep Survey (GOODS) spectroscopic observations in the Chandra Deep Field South (Vanzella et al. 2005, 2006, 2008, 2009a; Popesso et al. 2009) have accumulated, using the FORS2 and VIMOS instruments on ESO’s Very Large Telescope, spectroscopy of essentially all accessible sources. The source GDS J033218.92–275302.7 (GOODS J033218.92–275302.7, hereafter GDS18.92–02.7) was selected for the spectroscopic programme as a  $V_{606}$ -band dropout and has a blue  $i_{775}$ - $z_{850}$  colour due to a strong Ly $\alpha$  emission line falling in the  $i_{775}$ -band. It was subsequently studied in the context of SED fitting by Stark et al. (2007) and by Wiklind et al. (2008) who both conclude, on the basis of its apparently large Balmer break, that it is a high mass, old stellar population. Since the restframe UV images obtained with the ACS on HST show a very small angular size, the implication is that this is an

\* Based on observations made at the European Southern Observatory, Paranal, Chile (ESO programme 170.A-0788) *The Great Observatories Origins Deep Survey: ESO Public Observations of the SIRT Legacy/HST Treasury/Chandra Deep Field South.*; on observations obtained with the NASA/ESA Hubble Space Telescope obtained at the Space Telescope Science Institute, which is operated by the Association of Universities for Research in Astronomy (AURA), Inc.; and on observations made with the Spitzer Space Telescope, which is operated by the Jet Propulsion Laboratory, California Institute of Technology under a contract with NASA.

example of an ultradense spheroid at a very early epoch. A significant fraction of other Ly $\alpha$  emitters from GOODS, showing apparent Balmer breaks, have also been interpreted as evolved, massive stellar populations (Pentericci et al. 2009).

The presence of strong emission lines in the UV spectrum carries implications about the effect of nebular emission processes on the rest of the observable SED. There are circumstances in which the combination of nebular continuum from bound-free and two-photon emission together with emission lines can influence the appearance of, or even completely dominate, an underlying stellar population throughout the UV, optical and NIR spectrum. In this paper, we exploit the presence of a second emission line, identified as the [N IV], N IV] intercombination doublet at 1483, 1486 Å, to estimate the implied SED and compare with the extensive GOODS photometry of this object.

The presence of significant N IV] emission is rather rare in known astronomical objects. At low redshifts it is seen in some compact planetary nebulae and in peculiar very hot stars such as  $\eta$  Carinae (Davidson et al. 1986). It is also sometimes detected in AGN and quasar spectra but with an intensity that is low with respect to lines such as C IV and N V, although there are rare examples of “Nitrogen Loud” quasars that exhibit unusually strong nitrogen lines, e.g. Baldwin et al. (2003). At a redshift of 3.4, the Lynx arc (Fosbury et al. 2003, hereafter F03), is known to show N IV] with a strength comparable to other UV intercombination lines such as O III] and C III] and the resonance doublet C IV. This object is interpreted as an H II region ionized by very hot stars ( $T_{\text{eff}} \sim 80$  kK) with a nebular metallicity a few per cent of solar. In this case, the entire observed SED is nebular in origin and the stellar emission is not detected longward of Ly $\alpha$ . Glikman et al. (2007) report two N IV] emitting low luminosity “quasars” one of which, DLS 1053–0528 at  $z = 4.02$ , has an intensity ratio of N IV]/C IV = 1.9, a weak continuum and an SED which is considerably bluer than a typical quasar. This object has relatively narrow lines and may be more closely related to the Lynx arc than to an AGN.

In this paper we examine a sample of Ly $\alpha$  emitters from the GOODS spectroscopic data with redshifts spanning the range  $3.5 \leq z \leq 5.9$  and present new photometric measurements from the most recent releases of the HST, VLT and Spitzer imaging data. For our selected N IV] emitter, we use a photoionization modelling code to investigate the range of model nebulae that will produce the observed N IV] emission flux. Given the GOODS broad-band photometric measurements that extend from the *U*-band to the Spitzer MIPS 24  $\mu\text{m}$  channel, we calculate the contribution of the nebular line and continuum emission to these bands in order to constrain the nature of any non-nebular light that may contribute. In addition to modelling the SED of this one object, we address the possibility that nebular emission may contribute significantly to other sample members, a possibility that has already been suggested by Zackrisson et al. (2008). Our conclusions are of relevance to the interpretation of the SEDs of other high redshift Ly $\alpha$  emitters, where the emission line strength suggests that the nebula may be a significant contributor to the spectrum longward of the Ly $\alpha$  line. We adopt a cosmology with  $\Omega_{\Lambda} = 0.7$ ,  $\Omega_{\text{M}} = 0.3$  and  $H_0 = 70 \text{ km s}^{-1} \text{ Mpc}^{-1}$ . The *AB* magnitude system is used throughout.

## 2. Data

### 2.1. Sample

We have spectroscopically selected a sample of Ly $\alpha$  emitters from the publicly available data for the southern field of the

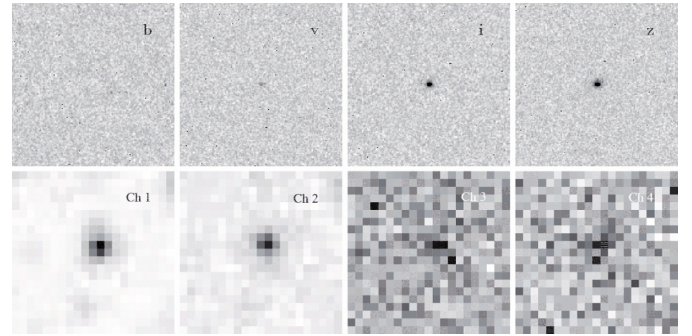


**Fig. 1.** Image cutouts of GDS18.92–02.7 from HST/ACS (top-row) and Spitzer/IRAC (bottom-row). The ACS stamps are 5 arcsec on a side and the IRAC stamps are 25.6 arcsec.

Great Observatories Origin Deep Survey (see Dickinson & GOODS Legacy Team 2001; Giavalisco et al. 2004, for a review of the GOODS project). The multi-wavelength observations provide us with information on the *U* (VLT),  $B_{435}$ ,  $V_{606}$ ,  $i_{775}$  and  $z_{850}$  (HST), *J*, *H*, *K*<sub>s</sub> (VLT), 3.6, 4.5, 5.8, 8.0 and 24  $\mu\text{m}$  (Spitzer) bands. Many other observations have been carried out, including deep integrations in the X-ray and radio domains from Chandra and the Very Large Array, respectively.

The spectroscopic observations carried out with the ESO VLT FORS2 instrument yield a wavelength coverage from approximately 0.55–1  $\mu\text{m}$  with a resolving power of  $R \approx 660$ . This programme has produced about one thousand redshift determinations between redshift 0.5 and 6.2, with more than one hundred Lyman break galaxies confirmed at redshifts beyond 3.5 (Vanzella et al. 2005, 2006, 2008).

From the GOODS data product archive <http://www.eso.org/science/goods>, we used the FORS2 online engine to select all the qf (quality flag) = A “emission” objects at  $z \geq 3.5$ . A few objects were excluded because of spectral contamination, one because it showed no Ly $\alpha$  emission and one because of positional uncertainty. This process yielded 23 objects from which an additional five were excluded due to large photometric errors in some passbands.

### 2.2. Photometry

Due to the different telescopes in use, the GOODS images are characterised by a large range in point spread function (PSF) dimension. An unbiased estimate of the colours is essential for analysis of the SED. We have used a PSF-matched photometric technique to obtain the *AB* magnitudes of each object in each band in a given aperture size. In the presence of potential contamination by neighbouring objects, we have used an optimum circular aperture which maximises the S/N of each object in all passbands simultaneously. For example, in the case of the match between ACS and groundbased *K*<sub>s</sub> or IRAC images, components may be clearly resolved by ACS but be merged in IRAC, or very red objects may be detected at the longer wavelengths but show no counterpart in the optical images. A curve-of-growth analysis yielded the optimum uncontaminated aperture.

Each source was examined in a  $12 \times 12 \text{ arcsec}^2$  cutout and a Monte-Carlo method used to estimate the background. The photometric measurements were made with SExtractor (Bertin & Arnouts 1996), where the background used was consistent with Monte-Carlo simulations. Finally, by selecting some bright but unsaturated stars near each galaxy, we computed the convolution kernel required to match the PSF of all the images to that

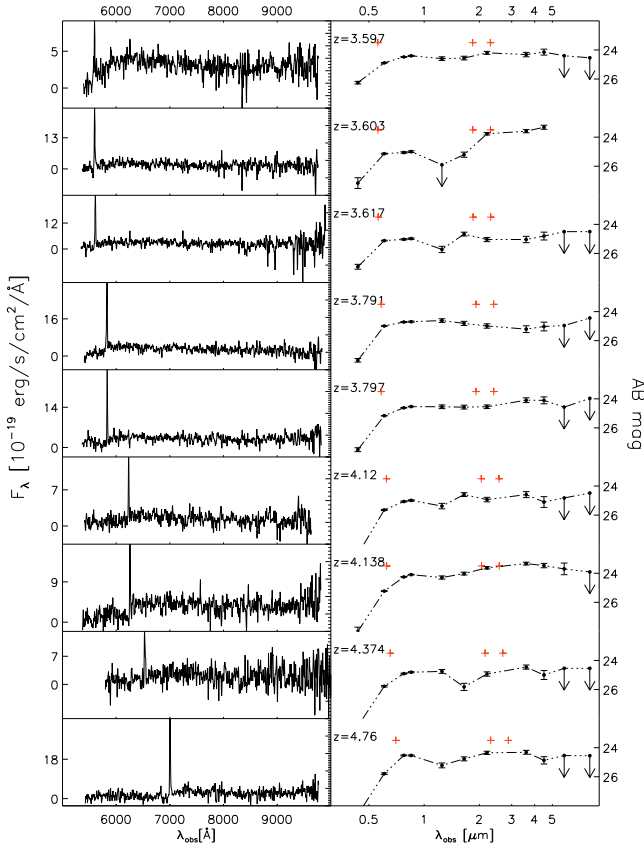


**Fig. 2.** FORS2 spectra and photometric SED – part 1 (redshifts 3.6–4.8). The photometric points are:  $B_{435}$   $V_{606}$   $i_{775}$  and  $z_{850}$  (HST),  $J_s$ ,  $H$ ,  $K_s$  (VLT), 3.6, 4.5, 5.8, 8.0 (Spitzer). The sources are presented in order of increasing redshift and so can be cross-referenced to Table 4. The (red) + “plusses” for each SED represent the wavelengths of Ly $\alpha$ , the 4000 Å Balmer break and the [O III] 5007 Å line. The photometric error bars are  $1\sigma$ .

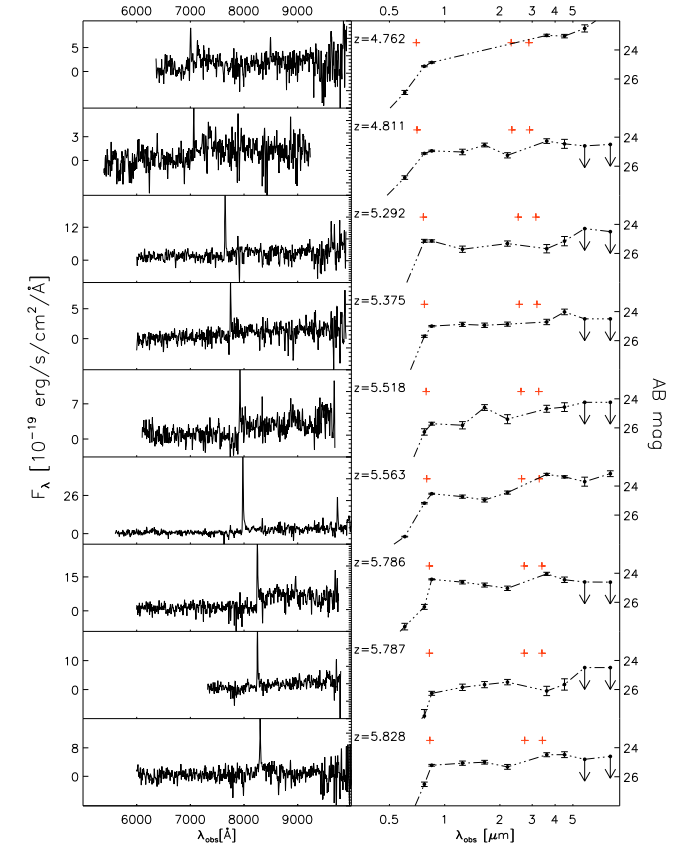


**Fig. 3.** FORS2 spectra and photometric SED – part 2 (redshifts 4.8–5.9).

with the largest. We generated about 200 PSF kernels of stars in different filters in order to find the best kernel using a  $\chi^2$  minimisation method. All magnitudes were corrected to a 6 arcsec circular aperture. The results for all bands appear in Table 4. We also use SExtractor to measure the “half-light” (or “effective”) radius of each galaxy in the  $z_{850}$ -band (also listed in Table 4).

### 2.3. The N IV] emitter

Of the 18 Ly $\alpha$  emitters in our sample, only one shows a clearly detected second emission line. Galaxy GDS18.92–02.7 with  $z_{850} = 24.5$ , was selected as a  $V_{606}$ -band dropout and has been confirmed to be at redshift 5.563 (redshift of the Ly $\alpha$  line uncorrected for absorption). The spectrum, included in Fig. 3 and shown in detail in Fig. 4, was extracted from several individual FORS2 multi-object masks and corresponds to a total exposure time of 14.4 ks (Vanzella et al. 2006). Detailed measurements of the spectrum of this object are presented in Vanzella et al. (2009b) and the parameters relevant to our modelling are summarised in Table 1.

The main spectral features are the Ly $\alpha$  emission line (rest-frame equivalent width ( $EW$ )  $\sim 60$  Å), the break of the continuum just blueward of the line, and the intercombination emission doublet [N IV], N IV] 1483.3, 1486.5 Å, whose intensity ratio can be used to estimate electron density (see Fig. 4). There is no clear detection of Si IV 1394, 1403 Å in absorption or emission nor of

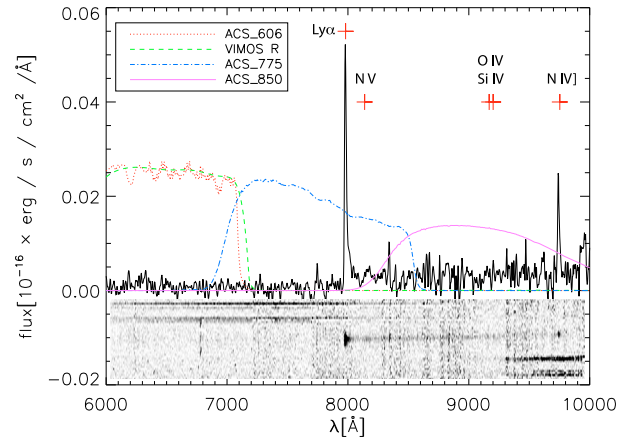


**Fig. 4.** FORS2 spectrum of source GDS18.92–02.7 showing the Ly $\alpha$  and N IV] emission lines and the ACS and VIMOS filter passbands. The expected positions of the NV, O IV and Si IV lines are also marked.

N V 1239, 1243 Å in emission. Vanzella et al. (2009b) also note that the object is extremely compact but marginally resolved in the ACS images.

## 3. SED modelling

In this section, we first discuss the modelling of GDS18.92–02.7. We then use a grid of similar photoionization models in order to assess the potential importance of nebular emission for interpreting the SED of the other sources in our sample.

**Table 1.** Summary of the physical quantities derived from the optical spectral features of GDS18.92–02.7.

Quantity	Value	Comment
$z$ (Ly $\alpha$ peak)	5.563	no abs. correction
$L$ (Ly $\alpha$ )	$3.8 \pm 0.3 \times 10^{43}$ erg s $^{-1}$	
$EW_0$ (Ly $\alpha$ )	$59_{-29}^{+195}$ Å (restframe)	89 Å with Ctm $_{\text{phot}}$
$z$ (N IV)]	5.553 (1486.5 Å)	high-density limit
$L$ (N IV)]	$1.3_{-0.4}^{+0.3} \times 10^{43}$ erg s $^{-1}$	
$EW_0$ (N IV)]	$22_{-10}^{+64}$ Å (restframe)	33 Å with Ctm $_{\text{phot}}$
$L$ (Si IV)	$\leq 0.11 \pm 0.07 \times 10^{43}$ erg s $^{-1}$	(1393.8, 1402.8 Å)
$L$ (N V)	$\leq 0.11 \pm 0.06 \times 10^{43}$ erg s $^{-1}$	(1238.8, 1242.8 Å)

**Notes.** Equivalent width values are also given using the continuum level derived from the photometry (Ctm $_{\text{phot}}$ ), taken from Vanzella et al. (2009b).

### 3.1. GDS J033218.92-275302.7

Two previous studies have attempted to fit the SED of GDS18.92–02.7 using the apparently large Balmer break to resolve the age-extinction degeneracy. Stark et al. (2007), using ID = 32\_8020, and Wiklind et al. (2008), as BBG 5197, both obtain an age of 0.9 Gyr, a stellar mass of close to  $10^{11} M_{\odot}$  and zero extinction. The latter authors, who use the two longer wavelength IRAC channels, 5.7 and 8.0  $\mu\text{m}$ , note that their fit is worsened by a deviant 5.7  $\mu\text{m}$  point.

Our nebular modelling is motivated by the realisation that a source with such strong emission lines in the FUV will necessarily have nebular contributions at longer wavelengths. Also, by analogy with the Lynx arc at the lower redshift of 3.4, it is possible that the significant jump in brightness between the  $K$ -band and the IRAC 3.6  $\mu\text{m}$  filter could be caused by strong [O III] 4959, 5007 Å emission lines producing an apparent, but false Balmer break signal. The nature of the photoionizing source can be inferred from the strength of N IV] and the non-detection of N V which also lies in a favourable region of the FORS2 spectrum. Again, by analogy with the arguments already used for the Lynx arc (F03; Binette et al. 2003; Villar-Martín et al. 2004), the limit on this line ratio can be used to argue for a hot blackbody-like source rather than the hard power law spectrum associated with an AGN. The absence of detectable radio (Kellermann et al. 2008) or X-ray (Giacconi et al. 2002) emission from the source at very low flux levels is also evidence against an AGN interpretation.

Since our modelling is designed to provide a “proof of concept” rather than a detailed SED fit, we use a set of blackbodies ranging from 60 to 120 kK as ionization sources. The use of hot stellar models having low or zero metallicity would have little effect on the gross properties of the predicted spectrum although they would be required to fit individual emission line fluxes if more observations were available. The *effective* temperature (the temperature of the black body which produces the same bolometric luminosity) of such stellar models would be somewhat lower (by  $\approx 10$ –15 kK) than the blackbody temperatures we use here.

The principal requirement of a model is to produce the observed luminosity of the N IV] doublet. The combination of density and ionization parameter,  $U$  (defined at the inner edge of the nebula) is constrained by the measured upper limit on the source size:

$$U = \frac{Q(\text{H})}{4\pi r_{\text{in}}^2 n_{\text{H}} c}$$

where  $Q(\text{H})$  is the rate of hydrogen ionizing photons radiated by the source,  $r_{\text{in}}$  is the inner radius of the cloud,  $n(\text{H})$  is the hydrogen number density of the cloud and  $c$  is the speed of light. Since, for all of our models, the depth of the ionized gas is small compared with the observed size of the source, we associate  $r_{\text{in}}$  approximately with the PSF-corrected measurement from the  $z_{850}$  ACS image of  $r_e$  (Table 4) which corresponds to 580 pc. The observed wavelength of N IV], compared with that of the blue-absorbed Ly $\alpha$  line, suggests that the doublet is emitted from a region that is in the high density regime (Vanzella et al. 2009b), show an enlarged plot of the spectrum of this region) with  $n_e \gtrsim 10^{4.5} \text{ cm}^{-3}$ , see: Osterbrock & Ferland (2006). We note, however, that in the Lynx arc, the density derived from N IV] doublet is significantly higher than the value of  $\lesssim 3000 \text{ cm}^{-3}$  derived from those of C III] and Si III] (Villar-Martín et al. 2004)<sup>1</sup>.

We use the photoionization code CLOUDY version 08.00 (Ferland et al. 1998) to calculate the models of H II regions exposed to the blackbody radiation. We assume an ionization bounded spherical geometry (i.e., the outer radius of the cloud is not defined) which means that the ionizing photon escape fraction is zero. The nebular gas is assumed to have constant density. From the output of the CLOUDY models, which includes both nebular continuum and line emission, we compute the theoretical magnitudes for all the photometric filters to compare with the GOODS observations.

We have calculated a grid of models exploring the parameter space of  $T_{\text{bb}}$  of the blackbody, the ionization parameter ( $U$ ) and the nebular metallicity ( $Z_{\text{neb}}$ ), investigating how the changes in these parameters affect the N IV] luminosity and the observed SED. We have assumed the solar relative abundances (as defined in CLOUDY) with the realisation that this is unlikely to be entirely appropriate at this epoch. In practice, this means that our calculated magnitudes will be affected by the abundance-dependent strength of lines from individual ions. The most important of these is the [O III] 4959, 5007 Å doublet that is included in the IRAC1 band. Note that, with the range of abundance considered here, oxygen is not the dominant coolant and so this emission line strength is proportional to abundance. Consequently, our principal assumption regarding abundances is that of a solar N/O ratio. Guided by the example of the Lynx arc, we have performed our modelling assuming that dust is not present. However, given the conclusions of the Ly $\alpha$  profile modelling discussed by Vanzella et al. (2009b), we do later examine the possibility of some dust extinction being present.

In addition to their fluxes, the emission line equivalent widths ( $EW$ ) are an important constraint because of their dependence on the strength of the continuum. In our models, the continuum under the N IV] line is dominated by hydrogen two-photon emission which becomes collisionally de-excited above an electron density of  $\sim 10^4 \text{ cm}^{-3}$ . The observed  $EW$  (Table 1) provides an additional constraint on  $T_{\text{bb}}$ ,  $U$ ,  $n_e$  and  $Z_{\text{neb}}$ .

Guided by the results of  $\chi^2$  testing of our model grid against the observed photometry and N IV] emission line flux, we choose a “fiducial” model that represents our best estimate for the model parameters (see Fig. 6). Because of our spectroscopic observation, high weight is accorded to the luminosity and the equivalent width of the N IV] doublet. This gives the parameters shown in Table 2.

It is significant to note that this is very close to the set of parameters as derived for the Lynx arc (F03) based on the fitting

<sup>1</sup> But note that, for the observed line ratio, the N IV] density in this paper should be  $10^5 \text{ cm}^{-3}$ , according to the method presented in Keenan et al. (1995), rather than the quoted  $2 \times 10^4 \text{ cm}^{-3}$ .

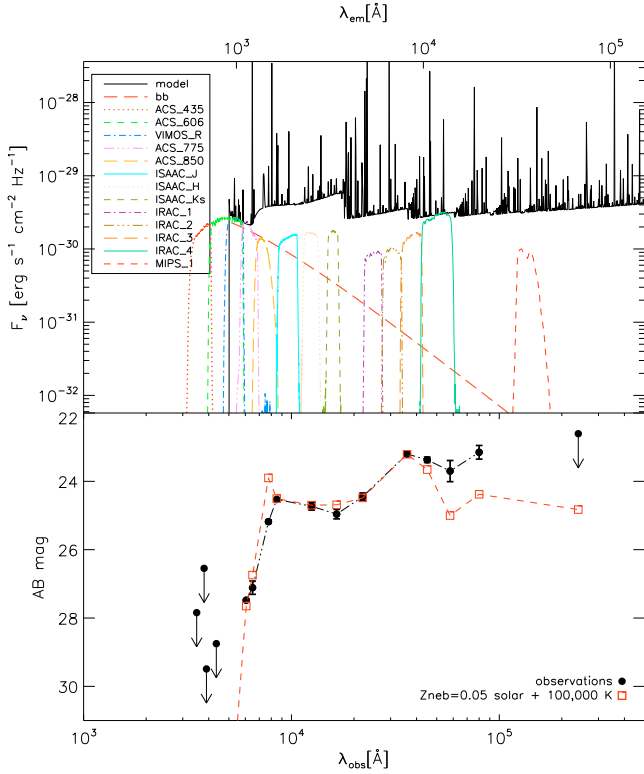


**Fig. 5.** Observed and modelled SED of GDS18.92–02.7. *Top panel:* the computed nebular spectrum from the fiducial model, the Rayleigh-Jeans tail of the ionizing blackbody spectrum and the GOODS filter passbands. *Bottom panel:* the observed and computed photometric SED. Additionally VIMOS *R* (VLT) and MIPS 24  $\mu$ m (Spitzer) magnitudes are included in the SED (Santini et al. 2009). The observed points have  $1\sigma$  error bars or are  $1\sigma$  upper limits. The points below Ly $\alpha$  have been corrected for IGM absorption. Our model does not model the Ly $\alpha$  radiative transfer and so the  $i_{775}$  point is really an upper limit. Note that the *Ks* band samples almost pure nebular continuum.

**Table 2.** Parameters of the fiducial photoionization model.

Parameter	Value	Unit
$T_{\text{bb}}$	100	kK
$\log(U)$	-1	
$Z_{\text{neb}}$	$0.05 Z_{\odot}$	
$Q(\text{H})$	$3 \times 10^{55}$	$\text{s}^{-1}$
$n_{\text{H}}$	$10^{2.9}$	$\text{cm}^{-3}$
$r_{\text{in}}$	$10^{21}$	cm

of many individual emission lines. There are differences in the assumed geometry and the particle density but these have only minor effects on the emitted spectrum. We have used a higher density in order to keep the nebula small enough to be consistent with the imaging data. The SED derived from this fiducial model is shown in Fig. 5 and the luminosities of some principal emission lines in Table 3. This model produces an HII region with an ionization structure and electron temperature distribution that results in an radially-averaged electron temperature of 23 kK.

In this model, the *Ks* band samples mostly nebular continuum while IRAC1 is dominated by very strong [O III] line emission resulting in a jump of 1.3 mag between restframe wavelengths of 0.33 and 0.54  $\mu$ m. The IRAC2 band is significantly influenced by H $\alpha$  and IRAC4 by He I 10 830  $\text{\AA}$ , this latter line becoming stronger at higher density (see the third panel of Fig. 6). Examination of Fig. 6 (which has 3- $\sigma$  error-bars) shows that

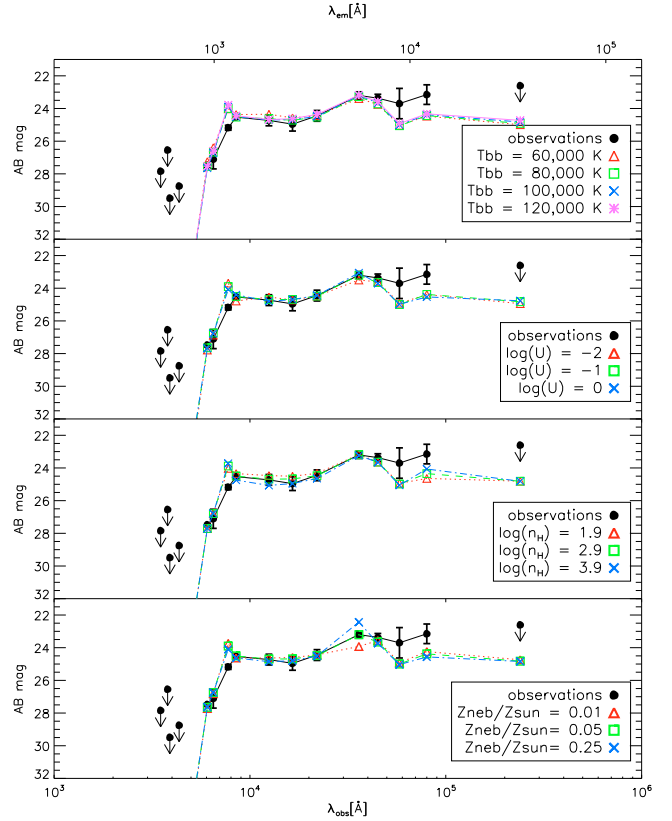


**Fig. 6.** As Fig. 5 but showing the effects of varying the four model parameters: *upper panel:*  $T_{\text{bb}}$ , *second panel:*  $\log(U)$ , *third panel:*  $\log(n_{\text{H}})$  and *lower panel:*  $Z_{\text{neb}}$ . Note the effect of metallicity on the IRAC1 band (due to [O III]) and the effect of the density on IRAC4 due to changes in the He I 10 830  $\text{\AA}$  line. To improve visibility in this plot, note that the error bars (but not the upper limits) are  $3\sigma$ .

**Table 3.** Fiducial model emission line spectrum.

$\lambda_{\text{rest}}$	$\log(L [\text{erg s}^{-1}])$	$I/I_{\text{H}\beta}$
O VI 1035	40.984	0.007
Si III 1207	41.589	0.026
Ly $\alpha$ 1215	44.724	36.011
N V 1240	42.229	0.115
Si IV 1397	42.564	0.249
O IV 1402	42.416	0.177
N IV] 1486	42.938	0.590
C IV 1549	44.054	7.698
He II 1640	43.026	0.7217
C III] 1909	42.985	0.657
[O II] 3727	41.411	0.018
He II 4686	42.127	0.0911
[O III] 5007	43.936	5.865
H $\alpha$ 6563	43.625	2.867

**Notes.** Note that no resonance line absorption is accounted for in these values. For the doublets, including [O III] 4959, 5007  $\text{\AA}$ , the number represents the sum of the two lines.

our fiducial model falls below the low signal/noise data from the IRAC3 and IRAC4 filters (see Fig. 1). The IRAC3 band in our model is dominated by bound-free continuum and is little affected by changing model parameters within the range we have considered. Although the IRAC4 band model also falls below the data, the amount can be lessened significantly by changing the density or adding a higher density component. Given the

marginal formal significance of these two discrepancies we do not consider it justified to attempt to add an additional source that would contribute flux at these wavelengths without destroying the fit at shorter wavelengths. In order to provide enough light from stars, the population would need to be old, massive and significantly reddened. Vanzella et al. (2009b) have examined SED fits using both single and mixed stellar population models. These both require an old,  $>700$  Myr for a single and  $\sim 400$  Myr for a mixed, massive,  $\sim 10^{11} M_{\odot}$ , population in order to provide the light seen in the IRAC bands. Such an addition would completely change the nature of the young, low-mass model we are proposing.

In addition to the requirement to explain the strength of the NIV] line, an important constraint is to not over-predict other emission lines within the FORS2 spectrum. The absence of NV 1243 Å has already been used to argue against an AGN-like ionizing continuum but it also limits the temperature of the blackbody to  $\leq 100$  kK. The O IV/Si IV complex from 1394–1413 Å increases in strength at the higher temperatures and is still predicted to be significant in our fiducial model (see Table 3). It is not seen in our data but, since we have no a priori information about the abundance of silicon, we do not consider this to be sufficient grounds for rejecting the model. The C IV resonance doublet is very close to the long wavelength limit of the observed spectrum and its detection is dependent on the effective redshift which can be influenced, like Ly $\alpha$ , by absorption. If it has the same redshift as NIV], the observational limit is below the prediction of our fiducial model by a factor of nearly 20 while if it is at the redshift of Ly $\alpha$  it would be undetected (as discussed by Vanzella et al. 2009b).

### 3.2. Sample modelling

The source GDS18.92–02.7 is the only member of our sample that contains a clearly detected second emission line in the FORS2 spectroscopy. There is, however, one source with groundbased IR spectroscopy that allows the measurement of [O II], [O III] and H $\beta$  line strengths. This is object CDFS 6664 (GDS J033233.33–275007.4) at a redshift of 3.791 from the AMAZE programme (Maiolino et al. 2008).

The presence of significant [O II] emission (i.e., comparable to H $\beta$ ) rules out the high temperature and high ionization parameter models that we need to explain strong NIV] emission. Since all of the spectra reported by Maiolino et al. (2008) do show [O II], their use of the locally calibrated  $R_{23}$  parameter and other line ratios to estimate metallicity is justified although it would not be for a NIV]-emitter, since it was not designed for the high ionization parameter cases. While we might expect the higher redshift sources to show evidence of hotter ionizing stars, the Lynx arc is at a similar redshift to the AMAZE sources but shows no [O II] and strong [O III] and NIV] lines. From Figs. 2 and 3, we see that most of our sample exhibit the rather flat spectra in  $f_{\nu}$ , that is a characteristic of the nebular models. However, without the evidence provided by emission line measurements in addition to Ly $\alpha$ , it is not possible for us to disentangle the stellar and nebular contributions. The relative importance of starlight and nebular emission in high redshift starforming galaxies has been discussed by Zackrisson et al. (2008) who model the effect of individual strong emission lines on multi-band SED observations. As we have confirmed, both with the Lynx arc and with GDS18.92–02.7 the [O III] lines can carry enough flux to affect significantly the magnitudes in even rather broad photometric bands and it is in the regime where its strength is proportional

to oxygen abundance. The presence of a significant excess flux in the band that includes these lines can be a hint that we are dealing with an SED with a significant nebular component.

## 4. Discussion

The model we employ for GDS18.92–02.7 is clearly rather rudimentary and is not expected to produce a detailed match to even the somewhat modest data set that we have. Simply summing models with a range of model parameters, notably density, would be more realistic and would tend to produce a better match to the observed SED at the longer wavelengths. However, the general properties of this kind of model are clear: the nebular continuum is approximately flat in  $f_{\nu}$  and is modulated by the presence of strong lines in particular photometric bands.

Although there appear to be no low redshift analogues of GDS18.92–02.7, the recent discovery of “Green Peas” by the Galaxy Zoo project (Cardamone et al. 2009) does, however, show that there exists a population of compact, strong [O III] emitting sources with high specific star formation rates, low metallicities and low reddening in the local universe. These sources demonstrate that vigorously star forming galaxies can exhibit SEDs with very significant nebular contributions to broad-band photometric measurements.

Arguments for thermal rather than non-thermal (AGN) photoionization were given in Sect. 3.1. It should also be noted that the upper limit on the MIPS 24  $\mu\text{m}$  flux (Table 4 and Fig. 5) excludes the steeply-rising SED from warm dust typical of AGN of types 1 and 2 (Miley & De Breuck 2008). Upper limits ( $3\sigma$ ) are available also on the MIPS 70 and 160  $\mu\text{m}$  fluxes of 2500 and 33 000  $\mu\text{Jy}$  respectively (Dickinson, priv. comm.; Coppin et al. 2009) but these values are, unfortunately, not strong discriminants. The source DLS 1053–0528 at  $z = 4.02$  discussed by Glikman et al. (2007) appears in a list of low luminosity type 1 AGN because its emission lines have a broad component with a  $FWHM > 1000 \text{ km s}^{-1}$ . However, aside from this characteristic, this object shares emission line and SED characteristics more closely with GDS18.92–02.7 and the Lynx arc than with typical AGN, notably the great relative strength of the nitrogen line with  $NIV]/CIV > 1$ .

The lower limit on the baryonic mass for our fiducial model is the sum of the masses of the ionizing stars plus the mass of the ionized nebula. To estimate the first of these components we use the zero metallicity models of Schaerer (2002) which give a value of  $Q(\text{H})$  per star. We choose his  $T_{\text{eff}} = 85 \text{ kK}$  model since it produces a similar ionization structure to our fiducial model. Such stars have a mass of  $50 M_{\odot}$  and  $Q(\text{H}) \sim 3 \times 10^{49}$  photons  $\text{s}^{-1}$ . Given the  $Q(\text{H})$  required for our model of  $3 \times 10^{55}$  photons  $\text{s}^{-1}$ , we need a million stars with a total mass of  $5 \times 10^7 M_{\odot}$ . The mass of ionized gas from the fiducial CLOUDY model is  $2.7 \times 10^8 M_{\odot}$ , giving a total minimum mass of  $3.2 \times 10^8 M_{\odot}$ , more than two orders of magnitude smaller than the stellar masses estimated by Stark et al. (2007) and Wiklind et al. (2008).

The need to properly include the nebular emission in high redshift starforming galaxies is not a new idea, e.g., Schaerer (2002); Zackrisson et al. (2008), but we believe that the Lynx arc at redshift 3.4 (F03) and GDS18.92–02.7 at  $z = 5.6$  are the only such objects known where the entire observed SED longward of Ly $\alpha$  may be contributed by nebular emission. The implication of this is that most of the stellar flux is emitted in the Lyman continuum. As shown by F03, a stellar population with a normal IMF that produces sufficient ionizing photons to produce the observed emission line fluxes would be easily detected

Table 4. Photometry ( $AB$  magnitudes) of sample sources in the GOODS passbands with their  $1\sigma$  errors.

GDS-id	$r_e('')$	$z$	IRAC4	IRAC3	IRAC2	IRAC1	K $s$	H	J	z	i	V	B
J033229.14-274852.6	0.138	3.597	-24.54	-24.40	24.15 $\pm$ 0.21	24.32 $\pm$ 0.15	24.20 $\pm$ 0.10	24.56 $\pm$ 0.13	24.60 $\pm$ 0.13	24.40 $\pm$ 0.13	24.48 $\pm$ 0.03	24.89 $\pm$ 0.02	26.25 $\pm$ 0.09
J033201.84-274206.6	0.169	3.603	...	...	23.32 $\pm$ 0.14	23.59 $\pm$ 0.11	23.77 $\pm$ 0.08	25.21 $\pm$ 0.18	-25.90	25.00 $\pm$ 0.06	25.06 $\pm$ 0.05	25.14 $\pm$ 0.03	27.16 $\pm$ 0.37
J033217.13-274217.8	0.127	3.617	-24.50	-24.50	24.80 $\pm$ 0.27	25.04 $\pm$ 0.22	25.04 $\pm$ 0.15	24.67 $\pm$ 0.13	25.72 $\pm$ 0.22	24.98 $\pm$ 0.22	24.98 $\pm$ 0.04	25.12 $\pm$ 0.03	26.92 $\pm$ 0.17
J033233.33-275007.4	0.138	3.791	-24.44	-24.96	25.03 $\pm$ 0.30	25.21 $\pm$ 0.23	24.99 $\pm$ 0.15	24.81 $\pm$ 0.14	24.62 $\pm$ 0.13	24.70 $\pm$ 0.04	24.72 $\pm$ 0.03	24.99 $\pm$ 0.02	27.35 $\pm$ 0.12
J033236.83-274558.0	0.153	3.797	-23.97	-24.57	24.11 $\pm$ 0.24	24.10 $\pm$ 0.16	24.55 $\pm$ 0.13	24.57 $\pm$ 0.13	24.55 $\pm$ 0.13	24.54 $\pm$ 0.02	24.62 $\pm$ 0.02	25.16 $\pm$ 0.02	27.50 $\pm$ 0.14
J033240.38-274431.0	0.111	4.12	-24.48	-24.82	25.10 $\pm$ 0.37	24.59 $\pm$ 0.21	24.93 $\pm$ 0.15	24.59 $\pm$ 0.13	25.38 $\pm$ 0.19	24.99 $\pm$ 0.04	25.07 $\pm$ 0.03	25.64 $\pm$ 0.04	-28.70
J033234.36-274855.8	0.251	4.138	-23.91	23.70 $\pm$ 0.40	23.47 $\pm$ 0.15	23.34 $\pm$ 0.10	23.63 $\pm$ 0.08	24.03 $\pm$ 0.10	24.29 $\pm$ 0.11	24.10 $\pm$ 0.02	24.25 $\pm$ 0.02	25.23 $\pm$ 0.03	28.00 $\pm$ 0.29
J033248.24-275136.9	0.146	4.374	-24.54	-24.54	25.00 $\pm$ 0.31	24.46 $\pm$ 0.14	24.93 $\pm$ 0.15	25.82 $\pm$ 0.25	24.75 $\pm$ 0.13	24.81 $\pm$ 0.04	24.91 $\pm$ 0.03	25.78 $\pm$ 0.05	-28.51
J033257.17-275145.0	0.173	4.76	-24.55	-24.54	24.87 $\pm$ 0.25	24.32 $\pm$ 0.13	24.36 $\pm$ 0.11	24.77 $\pm$ 0.14	25.22 $\pm$ 0.17	24.54 $\pm$ 0.03	24.53 $\pm$ 0.03	25.79 $\pm$ 0.06	-28.60
J033229.29-275619.5	0.156	4.762	21.31 $\pm$ 0.24	22.52 $\pm$ 0.25	23.05 $\pm$ 0.12	23.00 $\pm$ 0.08	...	...	...	24.86 $\pm$ 0.05	25.12 $\pm$ 0.04	26.93 $\pm$ 0.14	-28.86
J033210.03-274132.7	0.112	4.811	-24.5	-24.60	24.46 $\pm$ 0.31	24.27 $\pm$ 0.16	25.25 $\pm$ 0.18	24.54 $\pm$ 0.13	25.02 $\pm$ 0.19	24.94 $\pm$ 0.05	25.12 $\pm$ 0.05	26.78 $\pm$ 0.12	-28.61
J033221.30-274051.2	0.155	5.292	-24.5	-24.29	25.15 $\pm$ 0.32	25.68 $\pm$ 0.29	25.32 $\pm$ 0.18	...	25.71 $\pm$ 0.22	25.14 $\pm$ 0.08	25.13 $\pm$ 0.10	28.33 $\pm$ 0.25	-29.50
J033245.43-275438.5	0.190	5.375	-24.5	-24.50	24.02 $\pm$ 0.19	24.71 $\pm$ 0.18	24.86 $\pm$ 0.14	24.94 $\pm$ 0.15	24.88 $\pm$ 0.14	25.00 $\pm$ 0.05	25.70 $\pm$ 0.07	-28.97	-28.76
J033237.63-275022.4	0.263	5.518	-24.24	-24.24	24.57 $\pm$ 0.30	24.69 $\pm$ 0.24	25.40 $\pm$ 0.31	24.60 $\pm$ 0.20	25.82 $\pm$ 0.25	25.71 $\pm$ 0.10	26.28 $\pm$ 0.22	-29.50	-29.50
J033218.92-275302.7	0.109	5.563	23.15 $\pm$ 0.20	23.70 $\pm$ 0.31	23.37 $\pm$ 0.08	23.20 $\pm$ 0.07	24.45 $\pm$ 0.11	24.96 $\pm$ 0.14	24.73 $\pm$ 0.11	24.53 $\pm$ 0.04	25.18 $\pm$ 0.05	27.48 $\pm$ 0.03	-28.75
J033225.61-275548.7	0.110	5.786	-24.61	-24.60	24.45 $\pm$ 0.19	24.04 $\pm$ 0.11	25.04 $\pm$ 0.15	24.81 $\pm$ 0.14	24.61 $\pm$ 0.12	24.42 $\pm$ 0.04	26.32 $\pm$ 0.17	27.67 $\pm$ 0.23	-29.51
J033246.04-274929.7	0.120	5.787	-24.49	-24.49	25.65 $\pm$ 0.39	26.10 $\pm$ 0.32	25.49 $\pm$ 0.19	25.66 $\pm$ 0.21	25.85 $\pm$ 0.22	26.26 $\pm$ 0.14	27.83 $\pm$ 0.45	-29.08	-29.21
J033240.01-274815.0	0.120	5.828	-24.6	-24.80	24.48 $\pm$ 0.20	24.49 $\pm$ 0.14	25.32 $\pm$ 0.17	25.00 $\pm$ 0.13	25.07 $\pm$ 0.15	25.21 $\pm$ 0.06	26.52 $\pm$ 0.15	-29.65	-29.46

Notes. Negative numbers indicate upper limits. Also given are the half-light radii and the redshift measured from Ly $\alpha$ .

in the restframe UV. Unless we have a mechanism, such as a dust screen, that selectively absorbs this starlight in our line of sight, we are forced to the conclusion that we have a large population of stars with an effective temperature close to 100 kK. The absence of light from cooler stars implies that the cluster is either very young or has an intrinsically top-heavy IMF. The latter is an expectation for Population III stars. While we have no direct method to measure the *stellar* metallicity in these two objects, we do have estimates of the *nebular* metallicity of  $\approx 5\%$  solar. This may seem high compared with normal estimates for a Pop III environment (Bromm et al. 2001) but we need to better understand the rate of self-pollution within a cluster of a million stars in a deep potential well with temperatures around 80–100 kK and lifetimes of just a few million years.

Our modelling has been carried out without the inclusion of dust reddening. It is possible, however, to maintain a reasonable fit with the same model parameters other than an increased intrinsic luminosity (and total mass) by including  $E(B-V) \lesssim 0.1$  of Galactic dust for a screen model or  $E(B-V) \lesssim 0.2$  for a mixed model. The presence of some dust may be necessary to explain the Ly $\alpha$  profile (Vanzella et al. 2009b).

Once the need for a hot, thermal photoionization source is identified, it is natural to associate this solely with the presence of massive stars. Other sources of thermal radiation could be present, e.g., from shocks associated with a high supernova rate but, even if the entire kinetic luminosity of a core-collapse supernova  $\sim 10^{51}$  erg (Woosley & Weaver 1986) could be converted to Lyman continuum photons, this falls far short of the  $\sim 10^{54}$  erg of ionizing radiation emitted by a massive star during its lifetime (Schaerer 2002).

## 5. Conclusions

The possibility of starforming galaxies at high redshift, where very hot ionizing stars are expected, having restframe UV through MIR SEDs containing significant nebular contributions has been discussed for the last decade. The detection of emission lines in addition to Ly $\alpha$  provides, by using photoionization models, a way of quantifying this contribution. Compact objects containing very hot ionizing stars capable of producing lines such as N IV] and He II will also emit strong nebular continuum which we show can dominate the Rayleigh-Jeans tail from the ionizing stars. The presence of other strong lines falling within a photometric band can result in SED features than can be confused with jumps such as the Balmer break in conventional stellar population models. It is important to realise that the detection of a luminous emission line such as N IV] *necessarily implies* a substantial nebular contribution to the overall SED and therefore effectively excludes models which use purely stellar continuum contributions. The large equivalent widths of the emission lines can be used to limit the contribution of stars significantly cooler than 100 kK to the SED and so constrain the age of the cluster or its stellar IMF.

These highly ionized nebulae appear very different from the majority of H II regions in the local universe due to the higher temperature stars and higher ionization parameters. The restframe UV spectrum is rich with emission lines such as the intercombination doublets of C, N, O and Si which can be used for reliable abundance determinations.

Determined efforts with large groundbased telescopes equipped with efficient red and NIR spectrographs may allow us to observe some of the first stellar nucleosynthesis products from the young universe.

*Acknowledgements.* We thank Mario Nonino for so quickly finding this source in the GOODS spectroscopy after he had been tipped off about the importance of the N IV] line. Daniel Schaerer, Grażyna Stasińska and Daniel Pequinot gave us much useful modelling advice. We thank Francesca Matteucci for helpful discussions about the chemical evolution of galaxies. A.R. would like to thank Massimo Stiavelli for hosting her visit to STScI to learn and discuss matters pertaining to early star formation. In particular, we thank Eros Vanzella for his sterling work on the reduction and analysis of the GOODS/FORS2 spectroscopy and both he and Piero Rosati for many inputs to and discussions about this work.

## References

- Baldwin, J. A., Hamann, F., Korista, K. T., et al. 2003, *ApJ*, 583, 649
- Bertin, E., & Arnouts, S. 1996, *A&AS*, 117, 393
- Binette, L., Groves, B., Villar-Martín, M., Fosbury, R. A. E., & Axon, D. J. 2003, *A&A*, 405, 975
- Bromm, V., Kudritzki, R. P., & Loeb, A. 2001, *ApJ*, 552, 464
- Cardamone, C., Schawinski, K., Sarzi, M., et al. 2009, *MNRAS*, 399, 1191
- Coppin, K. E. K., Smail, I., Alexander, D. M., et al. 2009, *MNRAS*, 395, 1905
- Davidson, K., Dufour, R. J., Walborn, N. R., & Gull, T. R. 1986, *ApJ*, 305, 867
- Dawson, S., Rhoads, J. E., Malhotra, S., et al. 2004, *ApJ*, 617, 707
- Dickinson, M., & GOODS Legacy Team 2001, in *BAAS*, 33, 820
- Ferland, G. J., Korista, K. T., Verner, D. A., et al. 1998, *PASP*, 110, 761
- Fosbury, R. A. E., Villar-Martín, M., Humphrey, A., et al. 2003, *ApJ*, 596, 797
- Giacconi, R., Zirm, A., Wang, J., et al. 2002, *ApJS*, 139, 369
- Giavalisco, M., Ferguson, H. C., Koekemoer, A. M., et al. 2004, *ApJ*, 600, L93
- Glikman, E., Djorgovski, S. G., Stern, D., Bogosavljević, M., & Mahabal, A. 2007, *ApJ*, 663, L73
- Keenan, F. P., Ramsbottom, C. A., Bell, K. L., et al. 1995, *ApJ*, 438, 500
- Kellermann, K. I., Fomalont, E. B., Mainieri, V., et al. 2008, *ApJS*, 179, 71
- Maiolino, R., Nagao, T., Grazian, A., et al. 2008, *A&A*, 488, 463
- Miley, G., & De Breuck, C. 2008, *A&A Rev.*, 15, 67
- Nagao, T., Motohara, K., Maiolino, R., et al. 2005, *ApJ*, 631, L5
- Nagao, T., Sasaki, S. S., Maiolino, R., et al. 2008, *ApJ*, 680, 100
- Osterbrock, D. E., & Ferland, G. J. 2006, *Astrophysics of gaseous nebulae and active galactic nuclei*
- Ouchi, M., Shimasaku, K., Akiyama, M., et al. 2008, *ApJS*, 176, 301
- Pentericci, L., Grazian, A., Fontana, A., et al. 2009, *A&A*, 494, 553
- Popesso, P., Dickinson, M., Nonino, M., et al. 2009, *A&A*, 494, 443
- Santini, P., Fontana, A., Grazian, A., et al. 2009, *A&A*, 504, 751
- Schaerer, D. 2002, *A&A*, 382, 28
- Stark, D. P., Bunker, A. J., Ellis, R. S., Eyles, L. P., & Lacy, M. 2007, *ApJ*, 659, 84
- Vanzella, E., Cristiani, S., Dickinson, M., et al. 2005, *A&A*, 434, 53
- Vanzella, E., Cristiani, S., Dickinson, M., et al. 2006, *A&A*, 454, 423
- Vanzella, E., Cristiani, S., Dickinson, M., et al. 2008, *A&A*, 478, 83
- Vanzella, E., Giavalisco, M., Dickinson, M., et al. 2009a, *ApJ*, 695, 1163
- Vanzella, E., Grazian, A., Hayes, M., et al. 2009b, *A&A*, in press, [arXiv:0912.3007]
- Villar-Martín, M., Cerviño, M., & González Delgado, R. M. 2004, *MNRAS*, 355, 1132
- Wiklind, T., Dickinson, M., Ferguson, H. C., et al. 2008, *ApJ*, 676, 781
- Woolsey, S. E., & Weaver, T. A. 1986, *ARA&A*, 24, 205
- Zackrisson, E., Bergvall, N., & Leitert, E. 2008, *ApJ*, 676, L9